applied sciences

MDPI

Article

Loop-Type Field Probe to Measure Human Body Exposure to 5G Millimeter-Wave Base Stations

DukSoo Kwon, Young Seung Lee, Chang-Hee Hyoung, Jung-Hwan Hwang * and Hyung-Do Choi

Electronics and Telecommunications Research Institute (ETRI), 218 Gajeong-ro, Yuseong-gu, Daejeon 34129, Republic of Korea; duksoo@etri.re.kr (D.K.); lys009@etri.re.kr (Y.S.L.); hyoung@etri.re.kr (C.-H.H.); choihd@etri.re.kr (H.-D.C.)

* Correspondence: jhhwang@etri.re.kr

Abstract: This paper proposes a field probe to measure the power density (PD) at a millimeter-wave (mmWave) frequency band. The proposed probe is composed of a loop antenna in which one end is terminated with a load resistor. Such a structure enables the simultaneous measurement of electric (E)- and magnetic (H)-fields: the E-field is measured at a gap where the load resistor is placed, and the H-field is measured through the loop antenna. The simultaneous measurement makes it possible to measure PD for an incident wave even in the near field region where the E- and H-fields have different phases from each other. The proposed probe is fabricated and evaluated for its PD measurement performance. The measurement results show that the probe measures PD with an error less than 1.3 dB. Owing to the near field measurement, the proposed probe is useful in measuring the human body exposure to electromagnetic fields (EMFs) that are generated by 5G mmWave base stations.

Keywords: radiofrequency exposure; 5G; base stations; millimeter-wave measurements

Citation: Kwon, D.; Lee, Y.S.; Hyoung, C.-H.; Hwang, J.-H.; Choi, H.-D. Loop-Type Field Probe to Measure Human Body Exposure to 5G Millimeter-Wave Base Stations. *Appl. Sci.* **2023**, *13*, 11777. https://doi.org/10.3390/app132111777

Academic Editors: Salvador G. Garcia, Luis Manuel Diaz Angulo and Hai Lin

Received: 25 September 2023
Revised: 20 October 2023
Accepted: 25 October 2023
Published: 27 October 2023

1. Introduction

Many studies are being carried out to investigate effects of the fifth generation (5G) wireless communication on the human body since the 5G commercial service has started [1–7]. Especially for the 5G service using mmWave, human body exposure to electromagnetic fields (EMFs) from a base station is one of major concerns because base stations generate sharp beams and steer beams directly to 5G service users. The sharp beam results in a high power density (PD) to be exposed to the human body while the beam steering increases the possibility of such high-PD exposure. In [5], the mmWave exposure is studied in a cell level by exposing the cultured cells to the mmWave EMF. Refs. [6,7] investigated the EMF exposure in real environments by measuring PD from mmWave base stations.

5G mmWave base stations use millimeter waves in which the wavelength is very short. Due to this reason, the volume of the near field region is wide compared with that of the other base stations under 6 GHz. When the PD is measured in the near-field region, the E- and H-fields should be measured simultaneously because the two fields have different phase, which is a typical property of the near field. In this condition, the PD can be measured only when the E- and H-fields are measure simultaneously.

The PD is limited to be less than 20 W/m^2 over the mmWave band to protect the general public from EMF exposure [8]. The PD to be compared with the limitation is an average PD that is obtained by averaging PD samples within a 4 cm^2 area. Such spatial averaging is reasonable considering that a mmWave base station generates a sharp beam, and consequently, the PD can change sharply within a 4 cm^2 area. Previous studies used a horn or monopole antenna to measure PD generated from mmWave base stations [6,7]. Those studies measured the PD at a long distance of several dozens meters from base stations. Such a long distance makes the antenna beam spread widely, so the PD does not change much at adjacent measurement points in a 4 cm^2 area. General antennas are suitable to measure PD at a long distance from a base station. Within a short distance,

however, the antenna beam spreads less, and PD changes sharply within a 4 cm^2 area. In mmWaves, the field intensity changes significantly even with a small distance difference of several millimeters, so an array-type antenna is needed to measure PD [9,10]. Instead of antennas, a small-sized field probe having high spatial resolution is required for the exposure measurement of a 5G mmWave base station.

This paper proposes a small-sized probe to measure the mmWave exposure from a 5G base station. It provides high spatial resolution to measure PDs at a short distance from the base station. A probe structure and a processing circuit are designed and fabricated in a single printed circuit board (PCB). The fabricated probe is evaluated using a reference mmWave source that is defined in [11]. The proposed probe includes a loop antenna to measure PD. The utilization of the loop antenna is advantageous in that PD measurement is not affected by a feeding line connected to the antenna. The proposed probes can be arrayed within a 4 cm^2 area, so PDs can be measured at multiple points with a single measurement. Finally, the proposed probe is advantageous in measuring E- and H-fields at the same time and, consequently, can measure PD even in the near-field region.

2. Probe Design

2.1. Probe Structure

In [6,7], horn and monopole antennas were, respectively, used to measure PD from the 5G mmWave base station. Those antennas, however, have the disadvantage of a low spatial resolution because of the large antenna size. High spatial resolution is essential, especially for the exposure measurement of a mmWave whose wavelength is very small. A line antenna has been used for a field probe measuring exposure at radio frequencies much smaller than the mmWave. A typical example for the line antenna is the dipole or monopole one in [12,13]. Those line antennas have a short length much smaller than one wavelength at the measurement frequencies. Such a short-line structure suppresses any resonance, so the field probe has a flat frequency response over measurement frequencies. Also, it is possible to achieve a high spatial resolution for the exposure measurement.

When the line antenna is used to measure the mmWave exposure, its length is reduced to a few millimeters owing to its small wavelength. In this case, the antenna performance is affected by a feeding line that is connected to the line antenna. E-fields are coupled to a part of the feeding line in addition to the line antenna, so its effective length becomes larger than the original one. Such a length increase becomes critical at mmWave frequencies where the line antenna has is a length of only a few millimeters. The coupling to the feeding line is dependent on the length and the shape of the feeding line, so a different strength is measured depending on the feeding line even for the same E-field. Such unintended coupling increases the measurement uncertainty in an exposure measurement.

To resolve this problem, we propose a field probe with a loop antenna like in [14]. Figure 1 shows the loop antenna that is proposed in our study. Unlike the line antenna, the loop antenna experiences less coupling with the feeding line. This is because a closed loop is formed by the load resistor, as shown in Figure 1, while the feeding line makes no loop near the loop antenna. The incident H-field is coupled only with the loop antenna and induces a voltage at the load resistor. Such a coupling structure leads to less measurement uncertainty than a line antenna. The load resistor reduces the quality (Q) factor of the loop antenna and, consequently, suppresses any resonance resulting in a wideband operation of the probe.

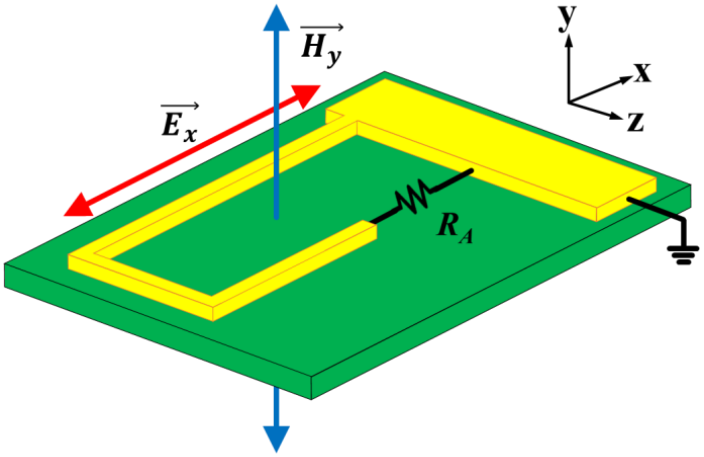

Figure 1. Structure of the 5G mmWave field probe.

As shown in Figure 2, the loop antenna is followed by the low-noise amplifier (LNA). Such a structure makes it easy to enhance the dynamic range of the field probe. The LNA amplifies the dissipating power at the load resistor, R_A, so the weak H-field causing low-power dissipation can be measured, resulting in a wide dynamic range. Our study used a commercial off-the-shelf (OTS) LNA for easy implementation [15]. Currently, no OTS LNA operating at mmWave frequencies supports a differential input. A passive-type balun can be used to transform the loop antenna output into the single-ended input for LNA. Such a balun, however, causes an additional signal loss in the signal path after the loop antenna. As shown in Figures 1 and 2, the loop antenna in our study has a single-ended output, so its output can be directly connected to the single-ended input of LNA. Like the LNA, a commercial OTS was used for a root mean square (RMS) power detector. As shown in Figure 2, the LNA is followed by the RMS power detector [16]. The RMS detector outputs a dc voltage, V_{PD}, proportional to PD of an incident wave, which will be explained later in this paper. The loop antenna is not a resonant one, so the operating bandwidth of the probe is determined by the LNA in which the bandwidth is about 13.5 GHz [15].

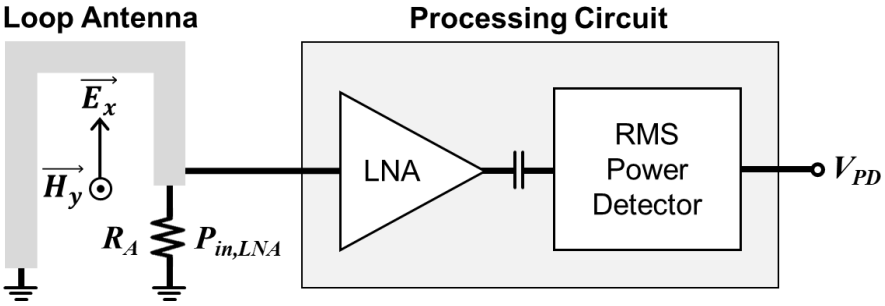

Figure 2. RF circuit after the loop antenna.

2.2. Probe Design

As shown in Figures 1 and 2, the loop antenna in the proposed has a singled-ended structure. The size of the loop antenna determines the resolution of the PD measurement. A smaller loop results in a high resolution of the PD measurement, but the coupling of the incident field with the loop decreases accordingly. The loop antenna is designed to have the resolution of a half wavelength at 28 GHz, so the loop has the longest length of about 5 mm.

The load resistor, R_A, in Figure 2 determines the receiving voltage of the probe. The load resistor also determines the resonance of the loop antenna. The load resistor is designed to avoid the resonance, so the frequency response of the loop antenna is close to being flat over a wide frequency band. Figure 3 shows the simulation results on the frequency response of the voltage at R_A for the increasing R_A. In the simulation, an elec-

tromagnetic wave having a PD of 10 W/m^2 is incident on the loop antenna. The voltage increases for the increasing R_A, so the LNA following the loop antenna generates a higher voltage at its output, resulting in high sensitivity of the probe. As shown in Figure 3, however, the increasing R_A results in fluctuation in the frequency response due to resonance. To avoid the resonance and to obtain a flat response, R_A is set to be 50 Ω.

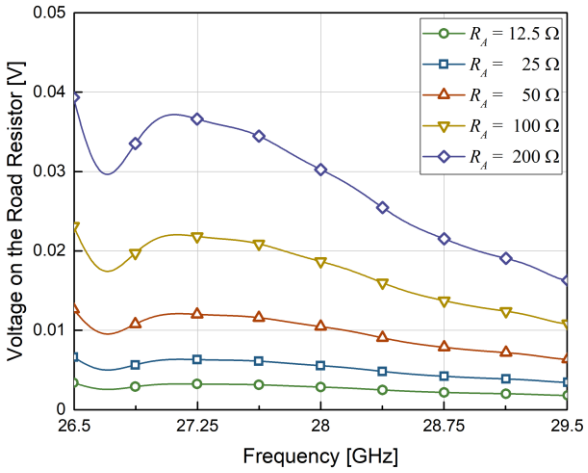

Figure 3. Frequency response of voltage at the load resistor, R_A.

2.3. Probe Operation

The single-ended loop shown in Figure 1 enables simultaneous measurement of the E- and H-fields. The H-field perpendicular to the antenna substrate is coupled to the loop antenna, and this coupling generates a current flowing through the load resistor. As shown in Figure 1, the loop antenna has a gap between the loop end and the ground plane. The E-field parallel to the antenna substrate is coupled to this gap, generating a voltage across the load resistor. The current and voltage then generate power that is dissipated at the load resistor. The load resistor also prevents the LNA from oscillating by creating a leakage path that avoids the radiation leakage [17]. Parallel distribution of the two resistors makes the input power to LNA equal to the dissipating power. Such an operation can be expressed as

$$P_{in,LNA} = C_E E_{x,RMS} \cdot C_H H_{y,RMS} \cos(\theta_E - \theta_H) \quad (1)$$

In (1), all coefficients have a phasor form. $P_{in,LNA}$ represents the input power to LNA, while $E_{x,RMS}$ and $H_{y,RMS}$ are the magnitude of the incident x-axis E- and y-axis H-fields, respectively, in the RMS unit. C_E is the coupling coefficient between the gap voltage end and the incident E-field, while C_H is that between the loop current and the incident H-field. The E- and H-fields can have different phases in the near field region. For increasing the difference between the phases, the power has a real component decreasing. In (1), θ_E and θ_H represent the phase of the E- and H-fields, respectively, and the cosine term, including the phase results in the real power component.

In Figure 2, LNA amplifies the input power in (1) with a gain of G_{LNA}. The amplified power is then applied to the RMS power detector. The detector converts the amplified power into a dc voltage that is proportional to the input power. This proportional relation is represented by another coefficient C_{PD}. The output voltage in a linear scale is proportional to the input power in dB units [16]. As a result, the output voltage V_{PD} is expressed using (1) as

$$V_{PD} = 10 \log[C_{PD} G_{LNA} C_E C_H \cdot E_{x,RMS} H_{y,RMS} \cdot \cos(\theta_E - \theta_H)] \quad (2)$$

In (2), $E_{x,RMS} H_{y,RMS} \cdot \cos(\theta_E - \theta_H)$ corresponds to PD of the incident field, so PD can be obtained by measuring V_{PD} and calculating PD from (2). The product of the coefficients in (2) can be obtained via measurement, which will be described later in this paper.

3. Probe Fabrication and Measurement

The proposed probe was fabricated in a single multi-layered PCB where the loop antenna was integrated with the LNA and the RMS power detector. After the fabrication, the probe performance was measured using a horn antenna as a reference source. The measured performance was compared with the simulated one.

3.1. Fabricated Probe and Measurement Setup

Figure 4 shows the fabricated probe for the 5G mmWave exposure measurement. The loop antenna has a size of 5.1 × 1.9 mm^2. The maximum length of the loop antenna is about half of a wavelength at 28 GHz; hence, the probe provides the spatial resolution of two points within one wavelength in the free space. The antenna substrate is composed of three layers, the total thickness of which is 800 µm. Each layer of the antenna substrate has a low tangent loss of 0.0024 at 10 GHz. The OTS LNA and the RMS power detector were attached on the substrate surface with resistor and capacitor components. As shown in Figure 4, the fabricated probe is terminated with the connector. This connector is to connect the probe to an interface board that reads the output voltage of the RMS power detector and controls the probe operation.

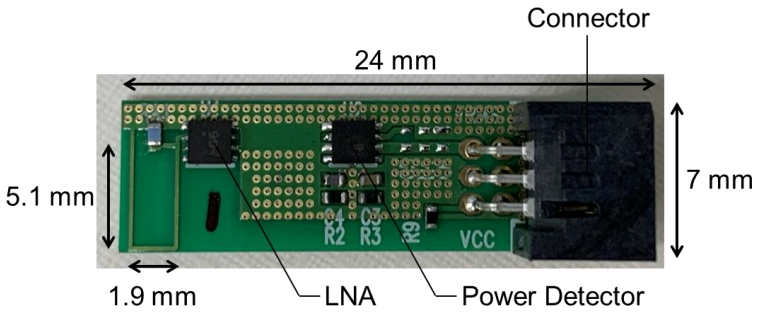

Figure 4. Fabricated 5G mmWave field probe.

Figure 5 shows the measurement setup to measure the performance of the fabricated field probe. The measurement setup includes the EMF radiator operating at 28 GHz. Our study used the reference antenna in [11] as the EMF radiator. As shown in Figure 5, the EMF radiator is the horn antenna in which the aperture has a slot array. EMFs radiated from the horn antenna with the slots are well analyzed in [11]. Numerical simulations can be performed to obtain PD in the free space, and the simulated PD is then compared with the measured one to evaluate the probe performance. The horn antenna with the slots in [11] is an EMF radiator to test the performances of a field probe that are used to measure PD on a surface of a mobile unit operating at 28 GHz. Such a test locates a field probe close to a mobile unit within several millimeters. In our study, however, the proposed field probe is used to measure PD from a base station at 28 GHz and, consequently, located at a longer distance from the EMF radiator, i.e., a 28 GHz base station. The horn antenna with the slots represents a 28 GHz base station well because it includes an array antenna which is composed of many dipoles or slots. Considering this point, the utilization of the horn antenna with the slot array is suitable to evaluate the probe for a 5G mmWave base station.

Figure 6 shows the measurement setup to measure the coefficients in (2) and probe performance, respectively. The coefficients include the effects of the radiation pattern of the loop antenna in the probe. The probe was horizontally aligned with the center of the horn aperture. As shown in Figure 5, the horn antenna was moved toward or away from the probe with the alignment condition maintained. The dc power supply provides dc voltages to operate the LNA and the RMS power detector composing the field probe. Figure 5 also shows the columns to place the field probe and the horn antenna, both of which are 50 cm above the bottom. The column for the horn antenna was clamped by the rail on the bottom and moved forward or backward along the rail to control the distance with the probe. The mmWave absorbers were placed at the bottom and all around to reduce any unintended reflections.

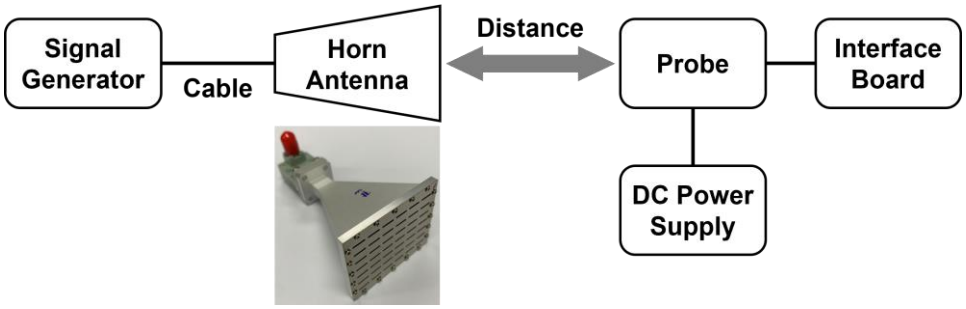

Figure 5. Configuration of the measurement setup.

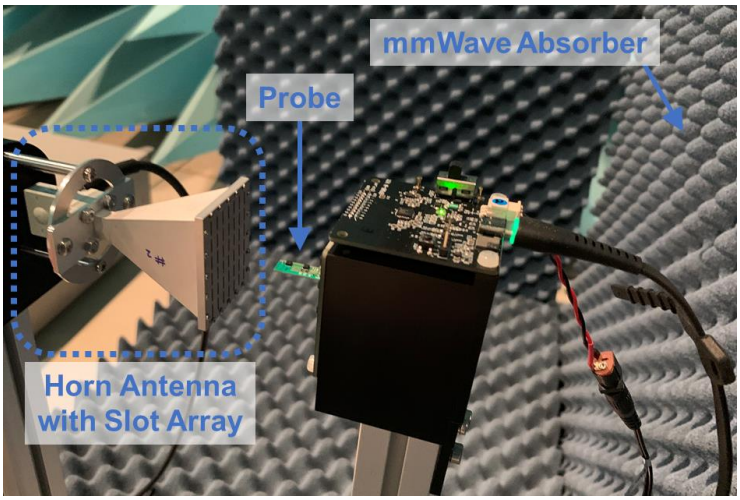

Figure 6. Measurement setup for fabricated 5G mmWave field probe with columns and rails to move the probe.

The product of the coefficients in (2) should be determined prior to the PD measurement. The product $G_{LNA}C_{PD}$ can be measured directly by measuring a response of the active-circuit path. For this, another PCB is fabricated by removing only the loop antenna and leaving the LNA and the RMS power detector. The active-circuit response can be measured by measuring the circuit output, i.e., the output voltage of the RMS power detector, by driving the circuit input with a 28 GHz signal with the power known. The active-circuit response is obtained by calculating the ratio between the input power and the output voltage. The calculated ratio corresponds to the product $G_{LNA}C_{PD}$. The calculated $G_{LNA}C_{PD}$ also includes any signal loss that occurs between the LNA and the RMS power detector.

Another product C_EC_H in (2) can be measured by applying a radiating field to the probe. The numerical simulation on the horn antenna calculates PD at a long distance from the antenna in the free space. Such a long distance makes PD able to be calculated in the far field, in which the E- and H-fields have the same phase: $\theta_E = \theta_H$. The radiating field with PD known from the simulation is applied to the probe, and the output of the RMS power detector is measured. In (2), the PD corresponding to the product of E and H is known from the simulation, while the product of $G_{LNA}C_{PD}$ is known from the previous active-circuit response. All other terms except C_EC_H in (2) are known, so C_EC_H can finally be calculated.

3.2. Measurement Results

The PD was measured at 28 GHz using the fabricated probe. Prior to the PD measurement, the coefficient product $G_{LNA}C_{PD}$ in (2) was measured using the probe with the loop antenna removed. The far-field measurement was then conducted to measure the coefficient product C_EC_H in (2). The coefficient product was measured using the horn antenna without the slot array. As shown in Figure 5, the front panel includes the slots. This front panel was temporally removed for the coefficient measurement. The panel removal expanded the far field region around the antenna [11]; hence, the coefficient measurement

could be conducted in the far-field region. Such a measurement generalizes the measured coefficient because the far field has a constant wave impedance and no difference in the phases of the E- and H-fields. The probe was placed about 1 m away from the horn antenna without the slot array. After driving the horn antenna with the signal generator in Figure 5, the output voltage V_{PD} was measured at the probe output. In (2), the PD corresponding to $E_{x,RMS}H_{y,RMS}$ was calculated from the simulation on the horn antenna in the free space. $(\theta_E - \theta_H)$ in (2) is equal to zero according to the measurement and the simulation in the far-field region. Finally, the coefficient product $C_E C_H$ in (2) was calculated using the measured $G_{LNA}C_{PD}$ and V_{PD} along with the simulated $E_{x,RMS}H_{y,RMS}$.

After calculating all the coefficients, the EMF was generated using the horn antenna with the slot array installed and the output voltage V_{PD} was measured at each distance. The PD was then calculated using (2). Figure 7 shows the measured PD for the distance increasing from the horn antenna with the slot array. The simulated PD is also shown in the same figure for the comparison with the measured PD. The PD was simulated in the free space at the same distance from the horn antenna with the slot array. As shown in Figure 7, the single probe measures PD close to the simulated one with the maximum error of about 3 dB. For the increasing distance, the decreasing rate is almost the same in the simulation and the measurement. Figure 7 shows the measured PD after rotating the probe by 90° on the axis that passes through the probe center in the longitudinal direction. As shown in Figure 7, the proposed probe has a polarization discrimination over 10 dB.

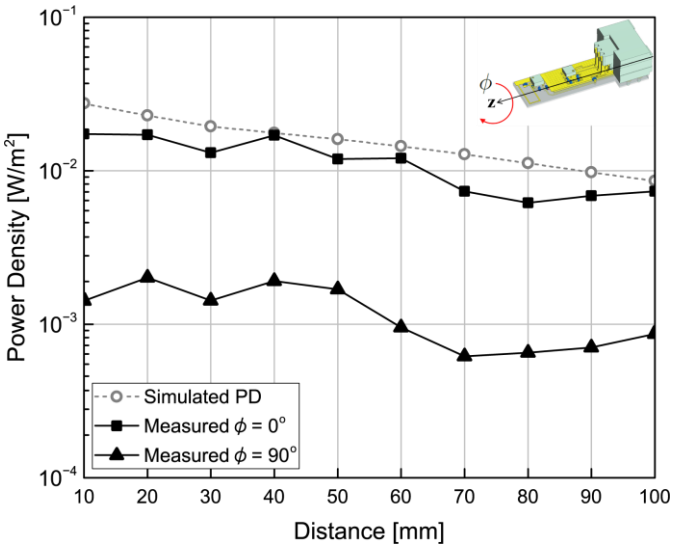

Figure 7. Power density measurement results of fabricated single probe.

3.3. Expansion to Probe Array

Owing to its small size, the single probe can be easily arrayed to measure PD at multiple points in the free space. Figure 8 shows the array probe in which a total of five single probes are assembled. Each probe is connected to the interface board through a right-angle PCB. As shown in Figure 8, the right-angle PCBs place the probes such that they have the same distance between them to transmit the output voltage of the RMS power detector to the interface board. The interface board displays PDs measured at each probe, in which PD is calculated using (2). The interface board also displays PD after averaging all measured PDs. As shown in Figure 8, all the loop antennas are inside the circular area that has 4 cm^2. According to [8], the PD limitation over 6 GHz should be compared with a PD that is averaged over 4 cm^2 area. For this, the PD should be repeatedly measured at multiple points to average all measured PDs. No other measurements, however, are required for the proposed array probe. Instead, a single measurement is enough to obtain the averaged PD.

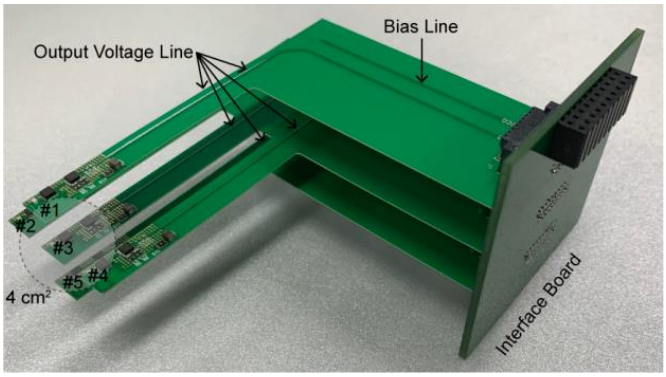

Figure 8. Probe assembled into array type.

Figure 9 shows the averaged PD for the same horn antenna with the slot array that radiates the accepted power of −16 dBm. For comparison, it also shows the simulated PD. The simulated PD was obtained by averaging PDs that were simulated at the same positions where each probe composing the array probe is located. As before, the proposed probe measures PD close to the simulated one with a maximum error of about 1.3 dB.

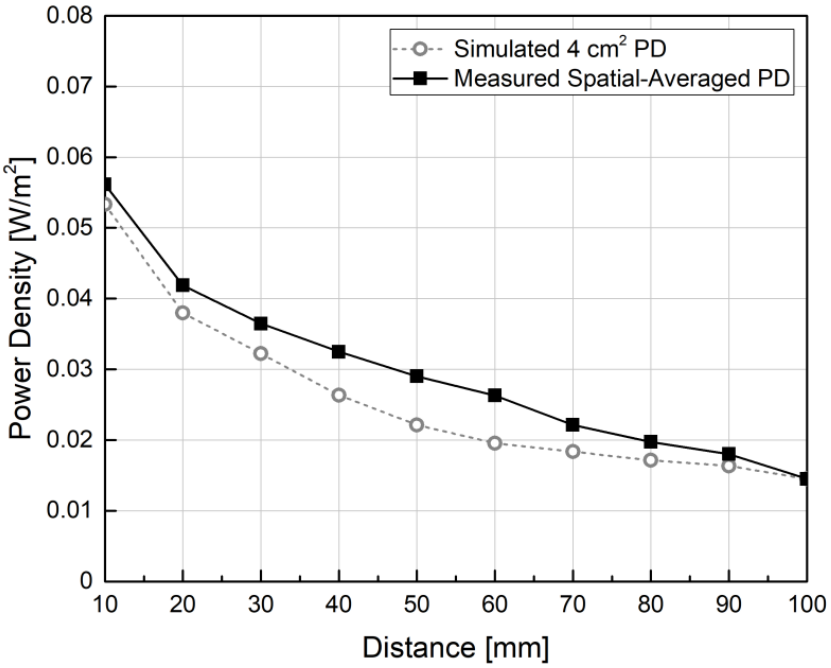

Figure 9. Power density measurement results of the probe array.

Figure 10 shows the measured frequency-dependent characteristics of the proposed probe array. We analyzed the changes in the probe output value when the proposed probe array receives frequency components other than 28 GHz. The proposed loop-type antenna is a non-resonant antenna that receives all frequency bands without impedance matching. Instead, the main factor causing the change is the probe output in the frequency response of the LNA gain of the processing circuit. The LNA used in the processing circuit has a flat gain in the mmWave band, so the change with frequencies at the same distance is insignificant [15]. However, in the near-field region close to the reference source, differences in the PD can occur due to the change in the length of the wavelength.

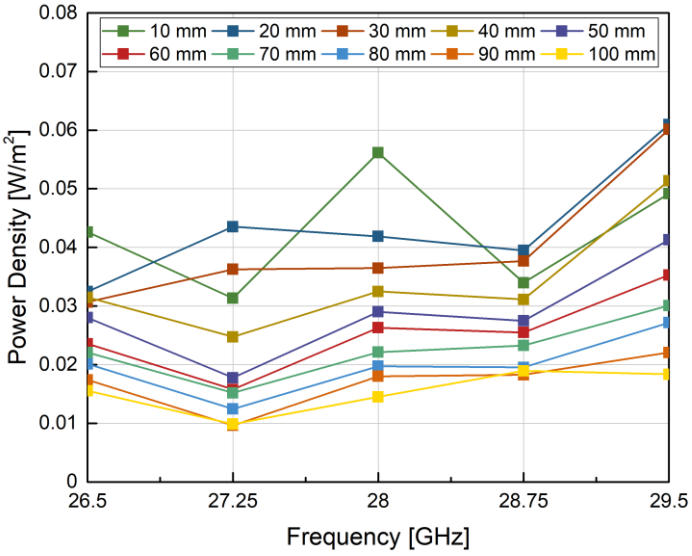

Figure 10. Measured power density sensitivity of the probe array with frequency.

4. Discussion on Reactive near Field Measurement

According to [11], the region where EMF is radiated from a source is divided into three regions: source regions I, II, and III. Source region III corresponds to the far-field region, while source regions I and II correspond to the near-field region. Source regions I and II have a different property with respect to the radiation characteristic: source region I is the reactive near-field region, while region II is the radiative near-field region. Ref. [11] provides equations to calculate the distances from a source to each region when the source is a linear array antenna. The horn antenna with the slot array corresponds to a linear array antenna, so the distances for the source regions can be calculated using the equations in [11]. According to those equations, the boundary distance between source regions I and II is about 2 mm from the horn antenna while the distance between source regions II and III is about 470 mm.

Considering this point, the measurement regions in Figures 7 and 9 are included in the radiative near field region. The measurement results in Figures 7 and 9 show that the proposed probe accurately measures the radiative near-field region. This is owing to the function of the proposed probe that measures the phase difference between the E- and H-fields as described in (2). As shown in Figure 1, the proposed probe provides the simultaneous measurement of the E- and H-fields using, respectively, the loop and the gap. As depicted in (2), this simultaneous measurement makes the phase difference be included at the output voltage V_{PD} of the probe. As a result, the proposed probe is useful in that PD can be measured even in the radiative near-field region with a single measurement, and consequently, it is not necessary to measure the E- and H-fields separately using two different probes like in [14].

5. Conclusions

This paper proposes the field probe to measure PD at the mmWave. The proposed probe has a structure to simultaneously measure the E- and H-fields, so PD can be measured even in the radiative near-field region. The measurement results and the comparison with the simulation results show that the proposed probe measures PD in the radiative near-field region with a maximum error less than 1.3 dB. The proposed probe can be used to evaluate human exposure to EMF generated by a 5G mmWave base station. Unlike other probes, the proposed probe measures PD even in the radiative near-field region; hence, the EMF exposure can be evaluated at a short distance from the base station, where such a short distance could increase PD beyond the limitation.

Author Contributions: Conceptualization, C.-H.H. and J.-H.H.; validation, Y.S.L.; investigation, D.K., C.-H.H. and J.-H.H.; writing—original draft preparation, D.K. and J.-H.H.; writing—review and editing, Y.S.L., J.-H.H. and H.-D.C.; visualization, D.K.; funding acquisition, H.-D.C. All authors have read and agreed to the published version of the manuscript.

Funding: This work was supported by Institute of Information & Communications Technology Planning & Evaluation (IITP) grant funded by the Korea government (MSIT) (2019-0-00102, A Study on Public Health and Safety in a Complex EMF Environment).

Institutional Review Board Statement: Not applicable.

Informed Consent Statement: Not applicable.

Data Availability Statement: Not applicable.

Conflicts of Interest: The authors declare no conflict of interest.

References

1. Aerts, S.; Verloock, L.; Van Den Bossche, M.; Colombi, D.; Martens, L.; Törnevik, C.; Joseph, W. In-situ measurement methodology for the assessment of 5G NR massive MIMO base station exposure at sub-6 GHz frequencies. *IEEE Access* **2019**, *7*, 184658–184667. [CrossRef]
2. Adda, S.; Aureli, T.; D'elia, S.; Franci, D.; Grillo, E.; Migliore, M.D.; Pavoncello, S.; Schettino, F.; Suman, R. A theoretical and experimental investigation on the measurement of the electromagnetic field level radiated by 5G base stations. *IEEE Access* **2020**, *8*, 101448–101463. [CrossRef]
3. Chiaraviglio, L.; Lodovisi, C.; Franci, D.; Pavoncello, S.; Aureli, T.; Blefari-Melazzi, N.; Alouini, M.-S. Massive measurements of 5G exposure in a town: Methodology and results. *IEEE Open J. Commun. Soc.* **2021**, *2*, 2029–2048. [CrossRef]
4. Lee, A.K.; Jeon, S.B.; Choi, H.D. EMF levels in 5G new radio environment in Seoul, Korea. *IEEE Access* **2021**, *9*, 19716–19722. [CrossRef]
5. Kim, K.; Lee, Y.S.; Kim, N.; Choi, H.D.; Lim, K.M. 5G Electromagnetic radiation attenuates skin melanogenesis in vitro by suppressing ROS generation. *Antioxidants* **2022**, *11*, 1449. [CrossRef] [PubMed]
6. Wali, S.Q.; Sali, A.; Allami, J.K.; Osman, A.F. RF-EMF exposure measurement for 5G over mm-wave base station with MIMO antenna. *IEEE Access* **2022**, *10*, 9048–9058. [CrossRef]
7. Colombi, D.; Ghasemifard, F.; Joshi, P.; Xu, B.; Di Paola, C.; Törnevik, C. Methods and practices for in situ measurements of RF EMF exposure from 5G millimeter wave base stations. *IEEE Trans. Electromagn. Compat.* **2022**, *64*, 1986–1993. [CrossRef]
8. International Commission on Non-Ionizing Radiation Protection. Guidelines for Limiting Exposure to Electromagnetic Fields (100 kHz to 300 GHz). *Health Phys.* **2020**, *118*, 483–524. [CrossRef] [PubMed]
9. Feng, Z.; Wang, J.; Diao, Y. Estimation of absorbed power density based on spherical wave expansion to plane wave expansion for exposure assessment at 30 GHz. *IEEE Antennas Wirel. Propag. Lett.* **2023**, *22*, 546–550. [CrossRef]
10. Xing, G.; Li, S.; Hoorfar, A.; An, Q.; Zhao, G. Near-field millimeter-wave imaging via multi-plane MIMO arrays. *IEEE Access* **2023**, *11*, 37347–37359. [CrossRef]
11. *IEC TR 63170:2018*; Measurement Procedure for the Evaluation of Power Density Related to Human Exposure to Radio Frequency Fields from Wireless Communication Devices Operating between 6 GHz and 100 GHz. Technical Report; International Electrotechnical Commission: Geneva, Switzerland, 2018.
12. Kanda, M.; Driver, L.D. An isotropic electric-field probe with tapered resistive dipoles for broad-band use, 100 kHz to 18 GHz. *IEEE Trans. Microw. Theory Techn.* **1987**, *35*, 124–130. [CrossRef]
13. Hwang, J.H.; Kwak, S.I.; Kwon, J.H.; Choi, H.D. Development of multi-band personal dosimeter for RF and ELF exposure monitoring. In Proceedings of the URSI Asia-Pacific Radio Science Conference (URSI AP-RASC), Seoul, Republic of Korea, 21–25 August 2016; pp. 414–416.
14. Shao, W.; Fang, W.; Huang, Y.; Li, G.; Wang, L.; He, Z.; Shao, E.; Guo, Y.; En, Y.; Yao, B. Simultaneous measurement of electric and magnetic fields with a dual probe for efficient near-field scanning. *IEEE Trans. Antennas Propag.* **2019**, *67*, 2859–2864. [CrossRef]
15. MAAL-011129 Broadband LNA, 18-31.5 GHz. MALCOM. Available online: https://www.macom.com/products/product-detail/MAAL-011129 (accessed on 20 April 2023).
16. LTC5596 Datasheet and Product Info: Analog Devices. Linear Technology. Available online: https://www.analog.com/en/products/ltc5596.html#product-overview (accessed on 20 April 2023).
17. Kwon, D.; Hwang, J.-H.; Hyoung, C.-H.; Choi, H.-D. A compact rectangular loop antenna for 5G mmWave application. In Proceedings of the International Symposium on Antennas and Propagation (ISAP), Sydney, Australia, 31 October–3 November 2022; pp. 203–204.